Effects of abnormal beams on writing qualities in massively-parallel e-beam systems

Md Nabid Hasan,[1] Soo-Young Lee,[1,a)] Byung-Sup Ahn,[2] Jin Choi,[2] Seom-Beom Kim,[2] and Chan-Uk Jeon[2]
[1]*Department of Electrical and Computer Engineering, Auburn University, Auburn, AL 36849*
[2]*Samsung Electronics, Mask Development Team, 16 Banwol-Dong, Hwasung, Kyunggi-Do 18448, South Korea*

(Received 27 July 2019; accepted 1 November 2019; published 19 November 2019)

While electron-beam (e-beam) lithography is widely used in transferring fine-feature patterns onto a substrate, its major drawback is the low throughput, especially for large-scale patterns. To increase the writing throughput, e-beam machines with massively-parallel beams were recently developed. In such a system, it is highly likely that some beams may not be normal, e.g., permanently on or off, a significant current fluctuation, beam-positioning error, etc. Therefore, it is crucial to understand how abnormal beams affect writing qualities. In this study, the effects of abnormal beams on the writing qualities are analyzed through an extensive simulation, comparing three different writing methods, *single-row writing I, single-row writing II, and multirow writing*, to suggest ways of reducing their negative effects. *Published by the AVS.* https://doi.org/10.1116/1.5121798

I. INTRODUCTION

Electron-beam (e-beam) lithography has been known for its capability to transfer complex and fine-feature patterns directly onto a substrate.[1–5] However, the main drawback of this maskless lithography technique is its low throughput, which limits its use for the fabrication of photomasks, in particular, of large size. One practical solution to the throughput limitation is to utilize multiple beams in a system. Recent developments in multibeam systems have offered improved productivity over the conventional technology (single variable-shaped-beam system), with a mask write time of less than 10 h.[6–10] In such a system (e.g., Multi-Beam Mask Writer-101),[6] there are a large number of beams, of which optimal use is critical to maximizing the efficiency of the system.

There can be various physical defects in the massively-parallel e-beam system. Physical defects include the dose deviation due to faulty beams, spatial and temporal fluctuations in beam current, beam deviating from its target position, etc. The impact of defective beams on writing qualities was not considered in the past. One recent paper[11] discussed briefly the effect of one faulty beam on the massively-parallel e-beam system. However, the main focus of this paper was on the effects of lithographic parameters, i.e., exposing interval, beam shape, etc., on different quality metrics, such as exposure fluctuation, line edge roughness (LER), maximum indent, etc. Also, this paper did not consider the nonideal conditions, for example, fluctuating beam current density, beam-positioning error, etc.

In this study, the effects of beam abnormalities on the writing qualities are analyzed for three different writing methods, namely, *single-row writing I, single-row writing II, and multirow writing*. In single-row writing method I or II,[12] the beam abnormalities can cause a significant exposure variation, line edge roughness, and maximum indent/outdent. On the other hand, the multirow writing method,[13] where each beam covers multiple rows of pixels in its respective writing path and each pixel is exposed by multiple beams, is able to reduce the negative effects of abnormal beams. The results from an extensive simulation are analyzed in detail, comparing the three writing methods in terms of the quality metrics.

The rest of the paper is organized as follows. In Sec. II, a model of the massively-parallel e-beam system is depicted along with the substrate system and transfer function. In Sec. III, the writing methods, single-row writing I, single-row writing II, and multirow writing, are described. In Sec. IV, the metrics of writing quality are introduced. In Sec. V, the simulation setup is explained. In Sec. VI, the simulation results are discussed, followed by a summary in Sec. VII.

II. MODEL

A. Massively-parallel electron-beam system

In a massively-parallel e-beam system (Fig. 1) like Multi-Beam Mask Writer-101,[6] a large number of beams are generated through a 2D array of apertures, each of which defines a beam. The beams can be individually turned on and off and are deflected in a synchronized manner, i.e., the same deflection angle for all beams. The substrate to be exposed can be modeled as an array of square-shaped pixels with size $B \times B$, the same as the beam size on the substrate (Fig. 1). The exposing interval, I_{ex}, can be larger, smaller, or equal to B. For simplicity, it is assumed that $I_{ex} = B$ throughout this paper.

B. Substrate system

In a typical substrate system[14] (Fig. 2), a resist layer is on top of the substrate, where the X–Y plane corresponds to the top surface of resist and the resist depth is along the

Note: This paper is part of the Conference Collection: The 63rd International Conference on Electron, Ion, and Photon Beam Technology and Nanofabrication (EIPBN 2019).
a)Electronic mail: leesooy@eng.auburn.edu

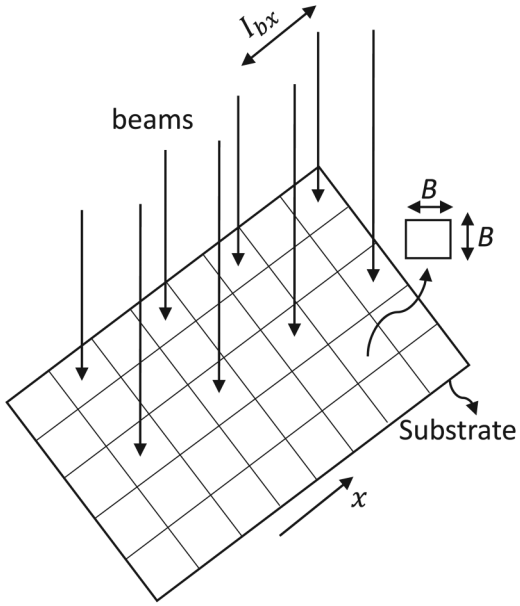

FIG. 1. Substrate moves in the x-direction exposed by parallel beams: the beam size is $B \times B$, and the beam interval is I_{bx}.

Z-dimension. The length and width of a feature are denoted by l and w, respectively. The 3D transfer function is denoted by $TF(x, y, z)$, describing the exposure distribution in the resist when a point (pixel) is exposed by a beam. Then, the 3D spatial distribution of exposure, $E(x, y, z)$, can be expressed by the following convolution:

$$E(x, y, z) = \int_{y'} \int_{x'} d(x - x', y - y')TF(x', y', z)dx'dy', \quad (1)$$

where $d(x, y)$ represents the dose distribution given by all beams.

C. Transfer function

The cross section of a beam is assumed to be of square in this study. As a beam travels from the electron source to the resist surface, the beam gets blurred.[15] Also, electrons experience scattering in the resist layer. Therefore, the transfer function is modeled by characterizing the beam blur and electron scattering, given a set of parameters (resist thickness, beam energy, etc.). The transfer function [Fig. 3(c)] is generated by convolving the ideal transfer function [i.e., constant within a square of $B \times B$, see Fig. 3(a)] with the

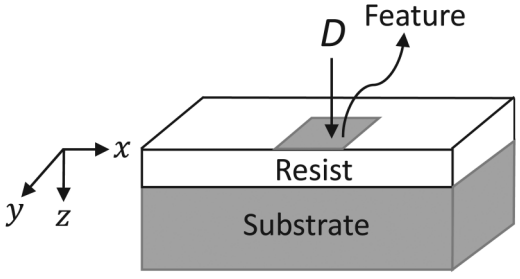

FIG. 2. Substrate system when the feature is exposed with a dose D.

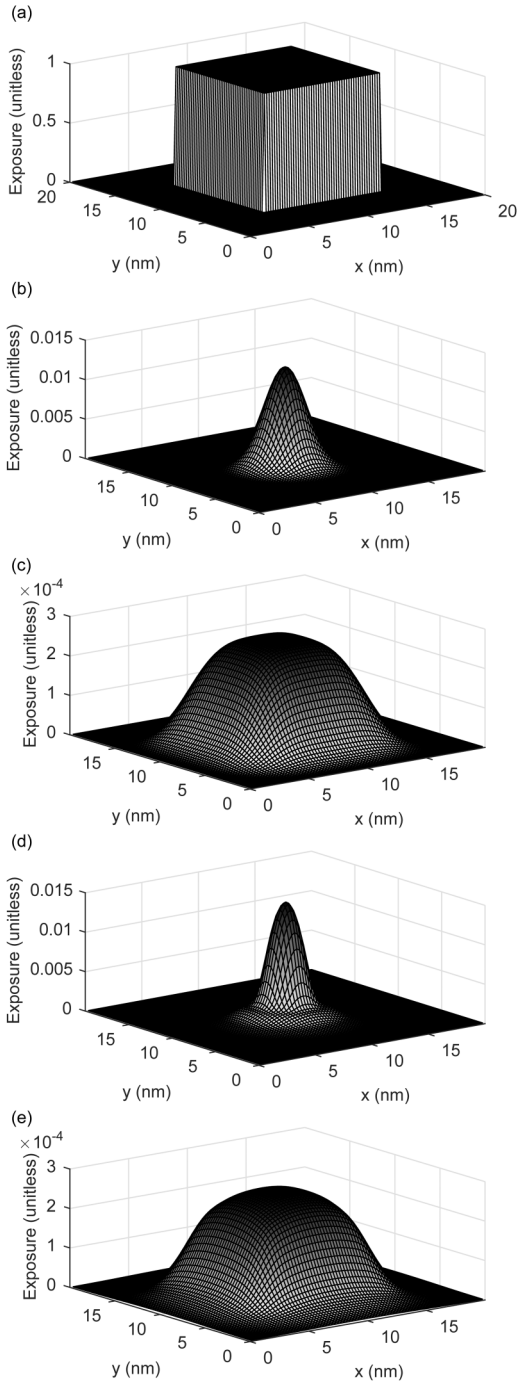

FIG. 3. (a) Ideal transfer function for the beam aperture of size $10 \times 10\,\text{nm}^2$, (b) the Gaussian function with $\sigma_t = 1.5$ nm, (c) the transfer function obtained from the Gaussian function in (b), (d) the PSF generated from the Monte Carlo simulation (SEEL) for the substrate system of 100 nm PMMA on Si and the beam energy of 30 keV: the estimated σ_t is 1.22 nm, and (e) the transfer function obtained from the PSF in (d).

Gaussian function [Fig. 3(b)], of which the standard deviation σ_t, to be referred to as *blurring factor*, quantifies the level of beam blur and electron scattering. Note that this Gaussian function is equivalent to the point spread function (PSF). A smaller σ_t results in a transfer function closer to the ideal one and leads to a lower level of proximity effect. Note that the blurring factor may be varied explicitly to study its effects on the writing quality.

The transfer function mainly models the forward scattering of electrons though the backscattering is partially represented by the long tail of the Gaussian function. However, the backscattering component of exposure has a very low amplitude and spatially varies slow. Therefore, the effect of the backscattering component on the writing-quality metrics (considered in this study, see Sec. IV) would be practically negligible. For comparison, the PSF generated from the Monte Carlo simulation (SEEL)[16] and the corresponding transfer function are also provided in Figs. 3(d) and 3(e), respectively.

III. WRITING METHODS

The three writing methods, single-row writing I, single-row writing II, and multirow writing, to be compared in terms of the effects of abnormal beams, are briefly described in this section. The dose a beam gives to a pixel in a *step* is denoted by d and the beam interval, the distance between two adjacent beams, is considered an integer multiple of B, expressed by $I_{bx}B$. All beams are controlled in a synchronized manner.

In single-row writing method I (Fig. 4), the writing path of each beam is on a single row of pixels. As the substrate moves continuously underneath the array of beams, each beam follows a pixel, being deflected in each step, to give a total (or target) dose of $D = n_s d$ to the pixel through n_s steps. The duration of n_s steps to give the target dose of D to each pixel is referred to as a *cycle*. Then, the beam is reset back to its vertical orientation and exposes another pixel in the next cycle. It is assumed that the time required to reset beams is much shorter than a step. The condition of $n_s = I_{bx} + 1$ is required to be able to achieve a uniform dose distribution without any hole in an exposed region. When a pixel is exposed by a (always-off) faulty beam, the pixel receives no dose, i.e., the dose reduction for the pixel would be $\Delta D = n_s d$. Each pixel may be exposed through more than one cycle using n_c sets of beams, where n_c is the number of cycles.

In single-row writing method II (Fig. 5), the writing path of each beam is still on a single row of pixels. But, the main difference from single-row writing method I is that each pixel is exposed jointly by a group of n_g consecutive beams, instead of a beam. This provides a better fault tolerance, decreasing the dose reduction by a faulty beam to $\Delta D = (n_s/n_g)d$. I_{bx} refers to the beam interval within each group of beams and I_{gx} the group interval which is the distance between groups. Note that beams need to be reset back to their vertical orientation after every (n_s/n_g) steps, i.e., n_g times per cycle.

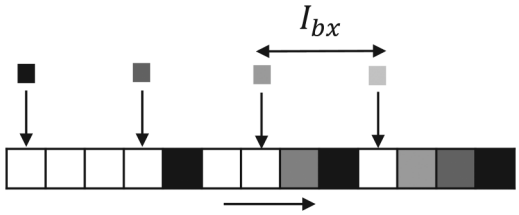

FIG. 4. Row of pixels (larger squares) being exposed by four beams (smaller squares) in single-row writing method I, where $I_{bx} = 3$ and $n_s = 4$, and the substrate moves to the right: this is a snapshot at the beginning of first step of a cycle. The pixels with the same shade of gray are exposed by the same beam with the corresponding shade.

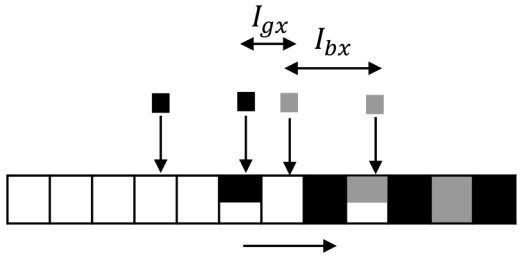

FIG. 5. Row of pixels (larger squares) being exposed by four beams (smaller squares) in single-row writing method II, where $n_s = 4$, $I_{bx} = 2$, $n_g = 2$, and $I_{gx} = 1$, and the substrate moves to the right. A group of two beams exposes each pixel and this is a snapshot right before the second beam in each group starts to expose the pixel partially exposed by the first beam. The pixels with the same shade of gray are exposed by the group of beams with the corresponding shade.

In the multirow writing method (Fig. 6), the writing path of each beam is over multiple rows of pixels and each pixel is exposed by a particular beam only once. That is, each beam exposes a set of n_s pixels, each pixel once, distributed over multiple rows. If the target dose for a pixel is $D = n_s d$, then it is exposed by n_s different beams in a row. Therefore, the dose reduction for a pixel due to a (always-off) faulty beam is minimized, i.e., $\Delta D = d$ independent of n_s. This method also enables the delocalization of the affected pixels. There can be more than one combination of selecting n_s pixels over multiple rows. In this study, the one shown in Fig. 6 is used, where the writing path consists of $I_{bx} + 1$ rows and each beam exposes one pixel from each row, being deflected n_s times in the diagonal direction.

IV. QUALITY METRICS

The abnormalities in the beams of massively-parallel e-beam system, such as always-off or always-on faulty beams, spatial and temporal beam current fluctuations, beam-

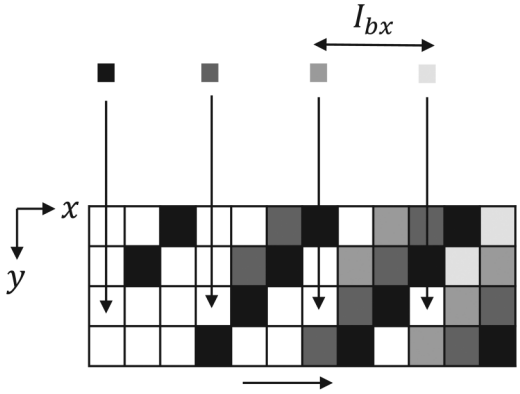

FIG. 6. Four rows of pixels (larger squares) being exposed by four beams (smaller squares) in the multirow writing method, where $I_{bx} = 3$ and $n_s = 4$, and the substrate moves to the right. This is a snapshot at the beginning of the third step of a cycle. The pixels with the same shade of gray are exposed by the beam with the same shade and each pixel is exposed by a beam, once in a cycle.

positioning error, etc., can cause a significant deviation from the desired spatial exposure distribution. This deviation may lead to a rough feature boundary. Therefore, for analyzing the effects of beam abnormalities on the writing qualities, a few quality metrics, such as the spatial exposure variation, critical dimension, line edge roughness, maximum indent, and maximum outdent, are considered. The quality metrics are described in this section.

A. Exposure variation

The exposure variation is defined as the standard deviation of exposure within a feature at a resist layer, excluding the exposure drop over the feature boundary [Fig. 7(a)],

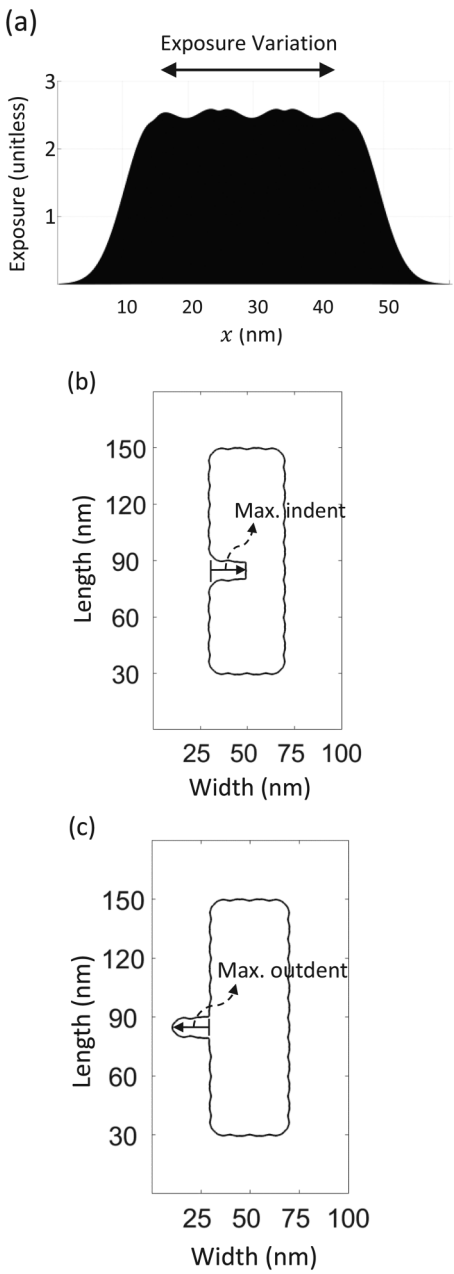

FIG. 7. Metrics of writing quality: (a) peak-peak exposure variation, (b) maximum indent, and (c) maximum outdent. The feature size is $40 \times 120\,\text{nm}^2$. $\sigma_t = 2\,\text{nm}$.

which is normalized to the average exposure. It can be expressed as follows:

$$E_{SD} = \frac{1}{\overline{E}}\sqrt{\frac{1}{wl}\int_{y=0}^{l}\int_{x=0}^{w}(E(x,y,z)-\overline{E})^2 dxdy}, \tag{2}$$

where $\overline{E}$ is the average exposure.

B. Line edge roughness

The LER is defined as the standard deviation of edge location along the length dimension of a feature at a resist layer, which can be expressed as follows:

$$\text{LER} = \sqrt{\frac{1}{l}\int_{0}^{l}(x_e(y)-\overline{x}_e)^2 dy}, \tag{3}$$

where $x_e(y)$ is the edge location and $\overline{x}_e$ is the average edge location.

C. Maximum indent and maximum outdent

Always-off faulty beams may introduce an exposure drop near the feature boundary, which can cause a large indent in the feature boundary. Such an indent is to be considered in addition to the LER since it can increase the resistance of a signal path directly. Hence, the maximum indent is defined as the largest edge deviation inward from the average edge location [Fig. 7(b)]. The maximum indent Δx_{in} can be represented as

$$\Delta x_{in} = \max_{y}(|x_{e,in}(y)-\overline{x}_e|), \tag{4}$$

where $x_{e,in}(y)$ is the edge location inside the average feature boundary.

Always-on faulty beams, exposing outside the feature boundary, can cause a significant resist development beyond the feature boundary, possibly causing a merge with a neighboring feature. Therefore, the maximum outdent is considered, which is defined as the largest edge deviation outward from the average edge location [Fig. 7(c)]. The maximum outdent Δx_{out} can be expressed as

$$\Delta x_{out} = \max_{y}(|x_{e,out}(y)-\overline{x}_e|), \tag{5}$$

where $x_{e,out}(y)$ is the edge location outside the average feature boundary.

V. SIMULATION

A feature of width 80 nm and length 320 nm is exposed by a massively-parallel e-beam system along its width dimension on a typical substrate system. The cross section of beam at the resist surface is $10 \times 10\,\text{nm}^2$ ($B = 10\,\text{nm}$), and the exposing interval I_{ex} is 10 nm ($I_{ex} = B$). The beam interval is 30 nm ($I_{bx} = 3$) and, therefore, the number of beams in one set is 4 ($n_s = I_{bx} + 1$). For single-row writing method II, n_g is set to 2.

For modeling the transfer function, a 3D point spread function is generated using a Monte Carlo simulation program SEEL for the substrate system of 100 nm PMMA on Si and the beam energy of 50 keV. From the point spread function, the total exposure and the forward scattering range are extracted in each of five resist layers which set the total exposure and blurring factor of the Gaussian function used to generate the transfer function of the respective layer through the convolution as described earlier.

The 3D exposure distribution in the resist is computed at the resolution, I_{sm}, referred to as *simulation interval*, which is set to $(1/4)$ nm so that a detailed analysis is possible. From the exposure distribution, the exposure variation is computed. The developing-rate distribution is derived from the exposure distribution, and then the remaining resist profile is obtained through a resist-development simulation.[14] The development simulation continues until the feature is fully developed to the bottom layer of resist. The dose is adjusted such that the width of developed feature at the middle layer is as close to the target width as possible when there is no abnormal beam in the system. From the resist profile, the critical dimension, LER, maximum indent, and maximum outdent are measured. The middle 80% segment of the feature is used in the computation of the metrics to exclude the edge effect (rounding at corners). Note that all the quality metrics are averaged over ten typical cases.

A massively-parallel e-beam system has a large array of beams, e.g., 512×512 beams. Though the probability p_b of a beam being faulty (always-on or always-off) is very small, the number of faulty beams in a system can be substantial. However, out of 128 beams required to expose the feature considered in this study, the average number of faulty beams is well under 1 for the realistic value of p_b. Therefore, in this analysis, the number of faulty beams affecting the feature, denoted by n_f, is considered instead of p_b.

The parameters that are varied when considering different beam abnormalities are described below:

Always-off and always-on faulty beams: The number of always-off or always-on beams n_f is varied from 0 to 5. Pixels in each writing path are exposed by one set of beams. Both the worst case (when n_f faulty beams are in the same row exposing adjacent pixels including a boundary pixel) and the best case (when none of the faulty beams exposes any boundary pixel) are considered. Also, to observe the effect of multiple sets of beams exposing each pixel, the number of sets of beams is varied from 1 to 5, while the number of faulty beams is kept at 1.

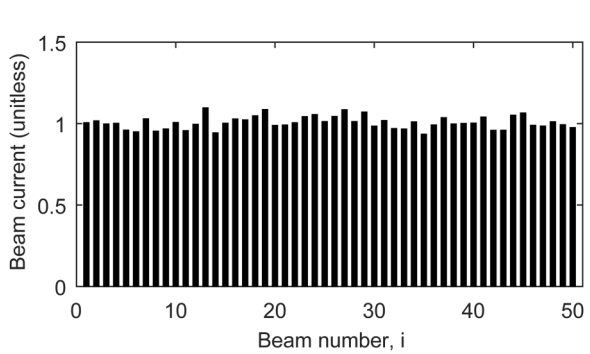

FIG. 8. Example of spatial fluctuation of beam current following the Gaussian distribution with an average of 1 and a standard deviation of 5%.

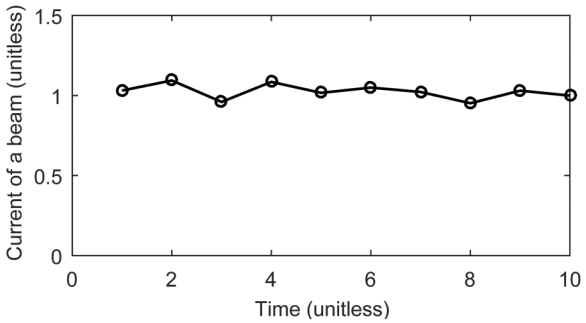

FIG. 9. Example of temporal fluctuation of beam current following the Gaussian distribution with an average of 1 and a standard deviation of 5%.

Spatial fluctuation of beam current: The beam current may not be the same for all beams (Fig. 8). This spatial fluctuation is assumed to follow a truncated Gaussian distribution with a standard deviation σ, where the maximum fluctuation is limited to 20% of the average current (or dose per step), and σ is varied from 0.5% to 10%.

Temporal fluctuation of beam current: The current of a beam may fluctuate with time (Fig. 9). This temporal fluctuation of beam current is also assumed to follow a truncated Gaussian distribution with a standard deviation σ, where the maximum fluctuation is limited to 20% of the average current (or dose per step), and σ is varied from 0.5% to 10%. The average currents of all beams are assumed to be the same to exclude the effect of spatial fluctuation.

Beam-positioning error: The actual point of exposure of a beam may deviate from its target position in both x and y directions (Fig. 10). The beam-positioning error in both directions is assumed to follow a truncated Gaussian distribution with a standard deviation σ and a maximum deviation of 5 nm from its center. σ is varied from 0 to 1 nm.

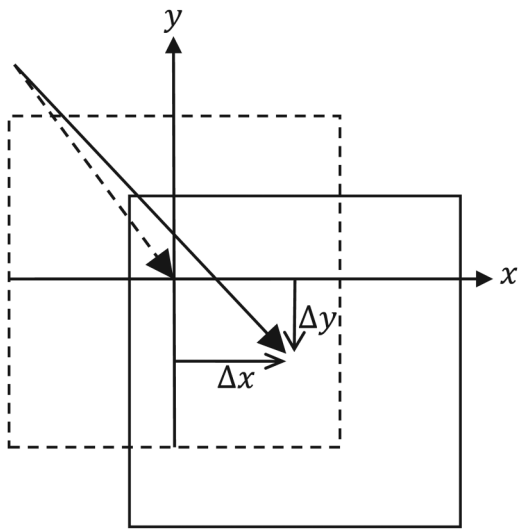

FIG. 10. Beam-positioning error. The dotted line represents the target exposure of a beam while the solid line represents the actual exposure of the beam deviating from the target position by $(\Delta x, \Delta y)$.

TABLE I. Summary of simulation setup.

Parameter	Value
Resist (PMMA) layer	Middle
Resist (PMMA) thickness	100 nm
Beam energy	50 KeV
Feature size	$80 \times 320\ \text{nm}^2$
Beam size, B	10 nm
Beam interval	30 nm
Total dose, D	$4d$
Blurring factor, σ_t	1–4 nm
No. of faulty beams, n_f	Varied from 0 to 5
Spatial and temporal beam current fluctuations	Gaussian; σ is varied from 0.5% to 10%
Beam-positioning error	Gaussian; σ is varied from 0 to 1 nm

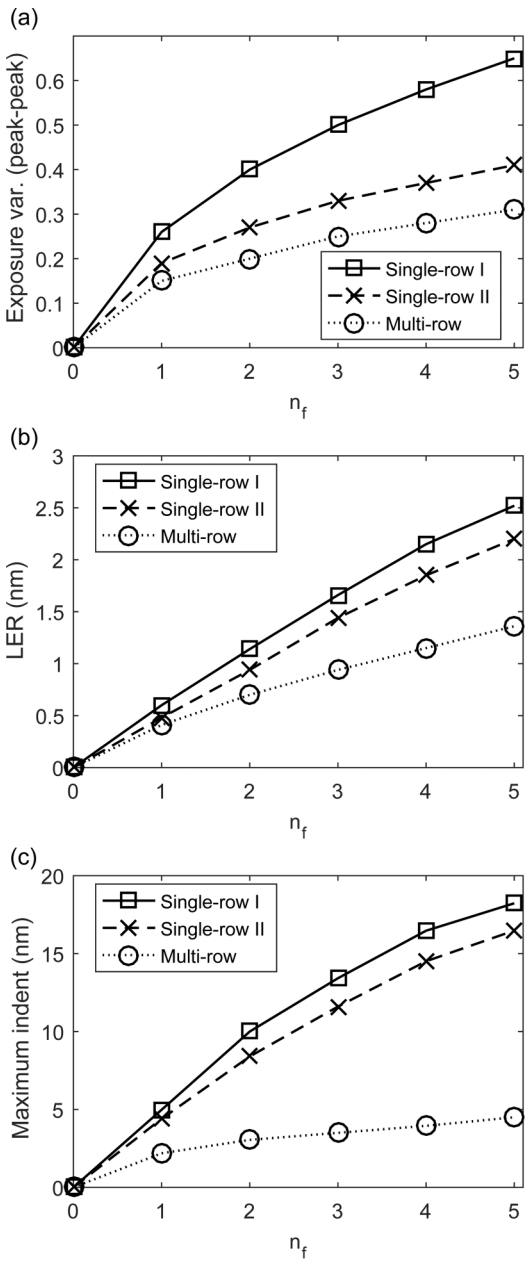

FIG. 11. (a) Exposure variation, (b) LER, and (c) maximum indent with the number of always-off faulty beams (n_f) varied. $\sigma_t = 2$ nm.

The values of all the parameters considered in this study are provided in Table I.

VI. RESULTS AND DISCUSSION

The simulation results considering only the always-off faulty beams are first presented. Then, the improvement by using multiple sets of beams is demonstrated. After that, the simulation results considering each of always-on faulty beams, spatial fluctuation of beam current, temporal fluctuation of beam current, and beam-positioning error are discussed separately. All the quality metrics are evaluated according to the respective equations in Sec. IV, at the middle layer of resist for $\sigma_t = 2$ nm except when σ_t is varied. The metrics show similar tendencies at other layers.

A. Always-off faulty beams

The simulation results of the three quality metrics obtained with n_f varied are provided in Fig. 11. As n_f increases, the exposure variation becomes larger due to the increasing number of affected pixels. A larger variation of exposure tends to result in a rougher feature boundary and more affected pixels close to the feature edges make an indent larger. Therefore, for a larger n_f, the LER and maximum indent become larger. It is also observed that all of the quality metrics are significantly improved by the multirow writing method, compared to both single-row writing methods. The main reason is that the dose reduction at a pixel due to faulty beams is lower in the multirow writing. Between the two single-row writing methods, the single-row writing method II performs better since the dose reduction is n_g times lower. Since n_g is set to 2 in the simulation setup, the affected pixels receive only 50% of the target dose and, therefore, remain mostly underdeveloped. As a result, the LER and maximum indent are not improved much by single-row writing method II. The feature contours in the remaining resist profiles obtained by the three writing methods when there is a faulty beam affecting edge pixels are compared in Fig. 12. It is clear that the maximum indent is significantly smaller for the multirow writing method.

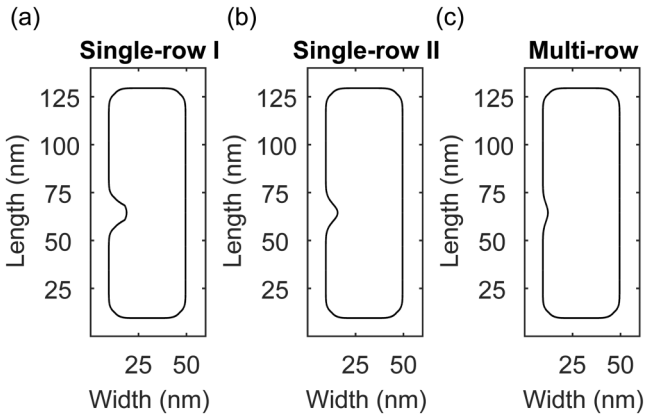

FIG. 12. Contour of a rectangular feature ($40 \times 120\ \text{nm}^2$) when a faulty beam affects edge pixels and $\sigma_t = 2$ nm: (a) single-row writing method I, (b) single-row writing method II, and (c) the multirow writing method.

B. Multiple sets of beams

From Fig. 13, it is seen that, as n_c increases, the exposure variation becomes smaller since the dose reduction at a pixel due to a (always-off) faulty beam is decreased by the factor of n_c. Also, the decreasing rate of exposure variation becomes lower with increasing n_c, since the percentage increase of the total dose at a pixel gets smaller as n_c increases. The LER and maximum indent also become smaller for a larger n_c. In Fig. 13, a large drop in the LER and maximum indent is observed for the multirow writing method when n_c is increased from 1 to 2 and for single-row writing method II when n_c is increased from 3 to 4. In both cases, the total dose received by the affected pixels is increased close to 90% of the target dose. Therefore, most parts of the affected pixels are developed, which improves the LER and maximum indent substantially. However, for single-row writing method I, even when $n_c = 5$, the affected pixels receive well below 90% of the target dose. Hence, the affected pixels remain mostly

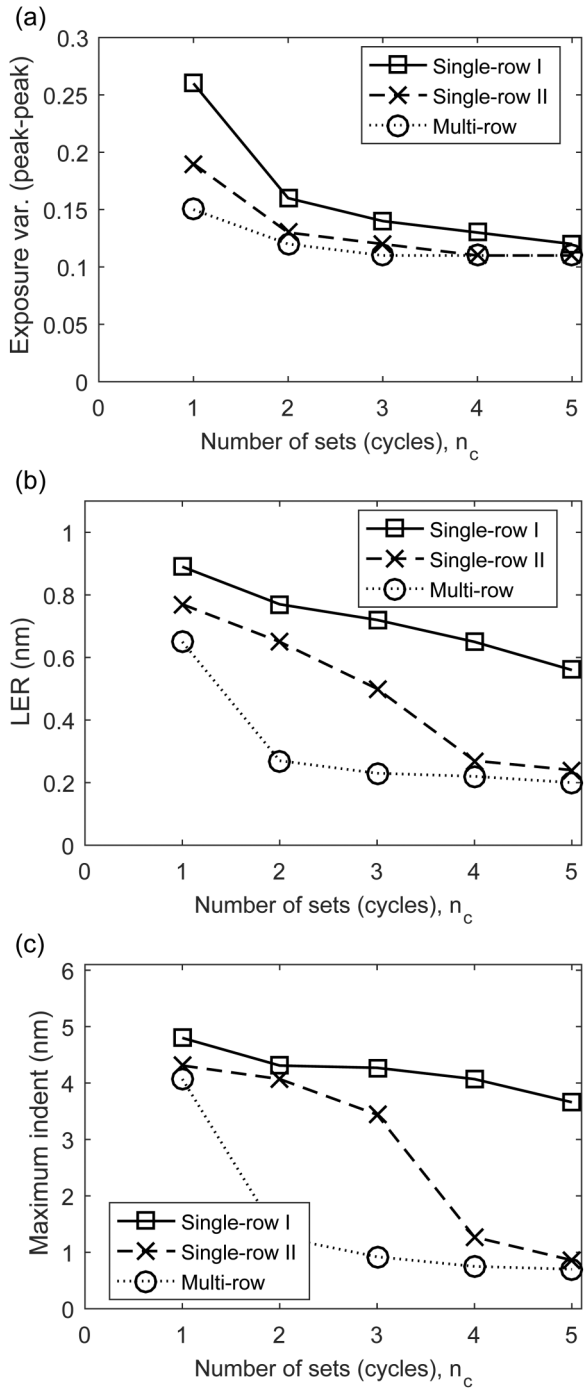

FIG. 13. (a) Exposure variation, (b) LER, and (c) maximum indent with the number of cycles (n_c) varied. $\sigma_t = 2$ nm, $n_f = 1$.

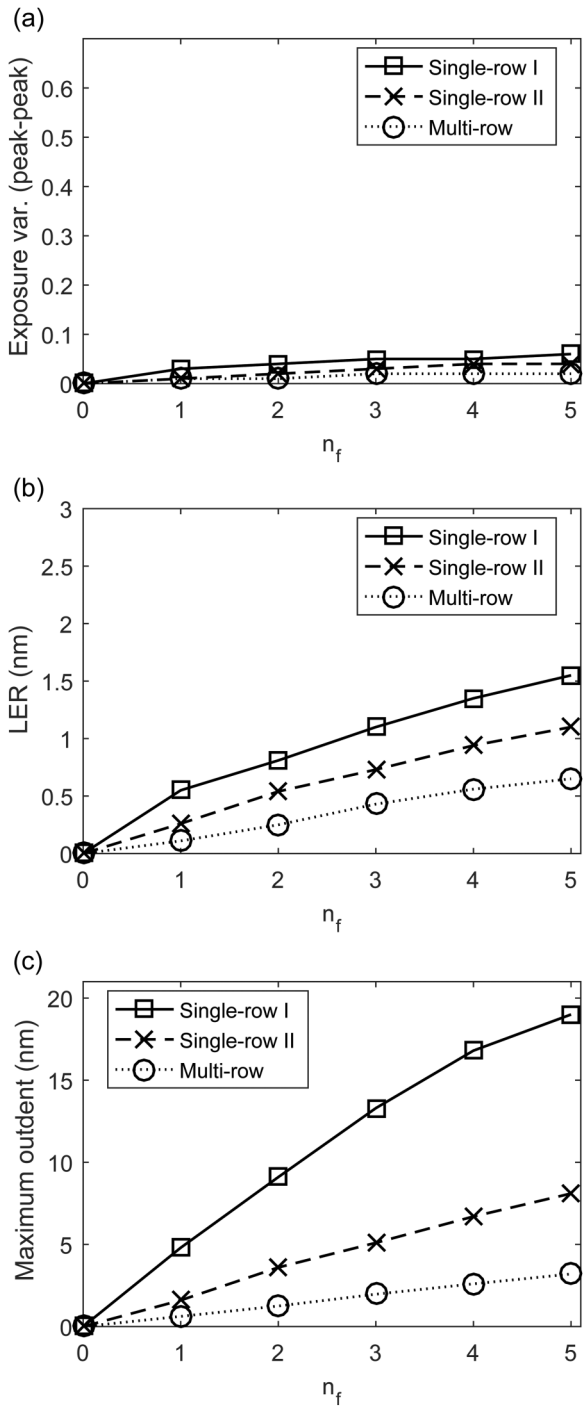

FIG. 14. (a) Exposure variation, (b) LER, and (c) maximum outdent with the number of always-on faulty beams (n_f) varied. $\sigma_t = 2$ nm.

underdeveloped, and the improvement in the LER and maximum indent is marginal, although the affected pixels get higher dose with increasing n_c.

C. Always-on faulty beams

The simulation results of the three quality metrics with the number of always-on faulty beams (n_f) varied are plotted in Fig. 14. The increase in the exposure variation with n_f is very small because always-on faulty beams do not affect the exposure distribution inside the feature boundary except edge pixels. However, the pixels affected by always-on beams just outside the feature boundary can contribute to the LER significantly, and consecutive affected pixels can make the outdent extremely large. In the single-row writing methods, each pixel is exposed by a beam multiple times. When the pixels just outside the feature boundary are exposed by an always-on beam, it causes the resist to develop well beyond the target boundary and results in a larger increase of the LER and maximum outdent. On the other hand, in the multirow writing method, each beam exposes a pixel only once and, therefore, the LER and maximum outdent due to always-on beams are smaller compared to both single-row writing methods.

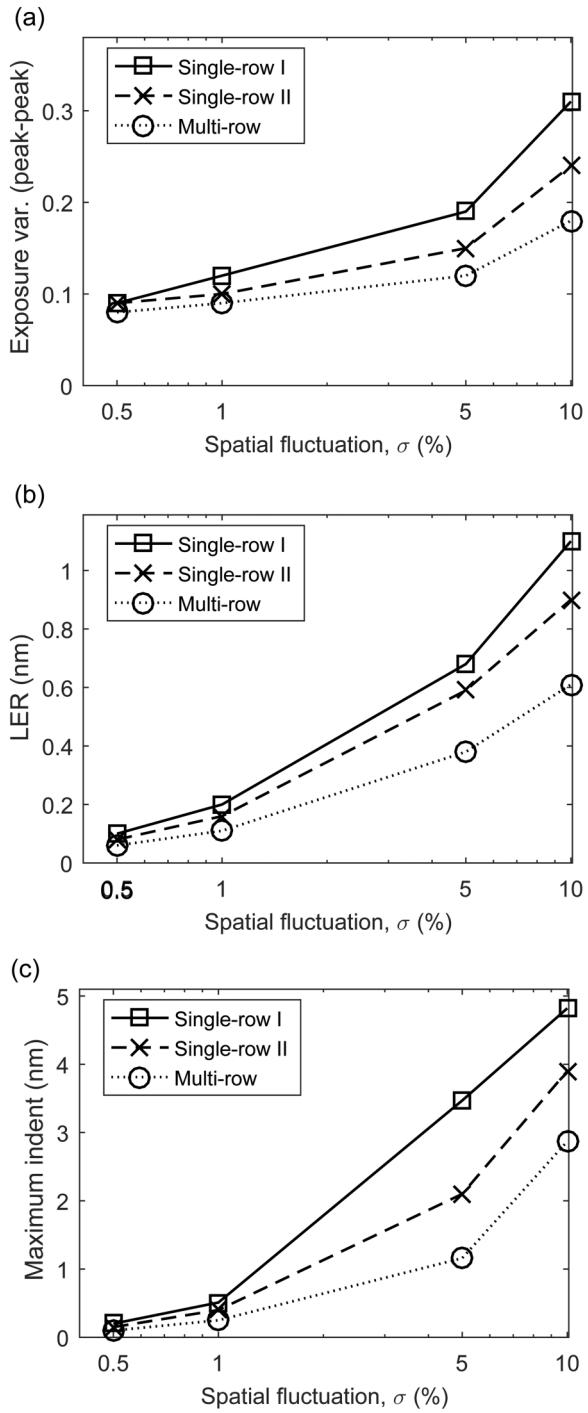

FIG. 15. (a) Exposure variation, (b) LER, and (c) maximum indent with the spatial fluctuation (σ) of beam current varied. $\sigma_t = 2$ nm, $n_f = 0$.

D. Spatial fluctuation of beam current

Figure 15 shows the effects of spatial fluctuation of beam current on the quality metrics. As the spatial fluctuation increases, the spatial variation of exposure becomes more significant, resulting in larger LER and maximum indent. Also, the improvement in the quality metrics by the multirow writing method compared to both single-row writing methods is notable. This is because, in the multirow writing method, each pixel is exposed by a larger number of beams than the single-row writing methods, and therefore different doses from multiple beams have a better chance to be averaged out. The number of beams exposing each pixel in single-row writing method II is n_g times larger than that in single-row writing method I, and therefore the quality metrics are significantly better for the former. The feature contours in the remaining resist profiles obtained by the three writing methods with a spatial fluctuation of beam current are compared in Fig. 16. Evidently, the edge of the feature is smoother for the multirow writing method.

E. Temporal fluctuation of beam current

In Fig. 17, the dependency of the quality metrics on the temporal fluctuation of beam current is shown. It is observed that all three metrics are the same for all three writing

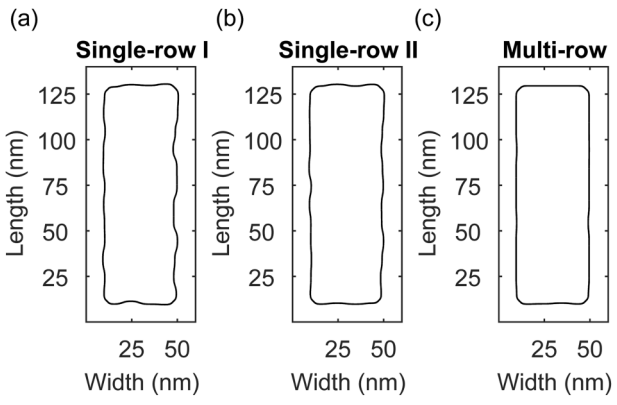

FIG. 16. Contour of a rectangular feature ($40 \times 120\,\text{nm}^2$) when the spatial fluctuation of beam current is 10% with no faulty beam and $\sigma_t = 2$ nm: (a) single-row writing method I, (b) single-row writing method II, and (c) the multirow writing method.

methods. In all three writing methods, each pixel is exposed the same number of times, either by one or multiple beams, leading to the same level of time-averaging of the temporal fluctuation. Another observation is that the metrics with the temporal fluctuation of beam current are substantially smaller than those with the spatial fluctuation for the single-row writing methods but not for the multirow writing method. This is because there is always a time-averaging effect when a pixel is exposed multiple times. But, for a pixel not exposed by multiple beams, there is no averaging effect to compensate the spatial fluctuation.

F. Beam-positioning error

The simulation results of the three quality metrics obtained with the beam-positioning error (σ) are given in Fig. 18. The more a beam deviates from its target position, the greater the exposure variation, LER, and maximum indent. Also, all

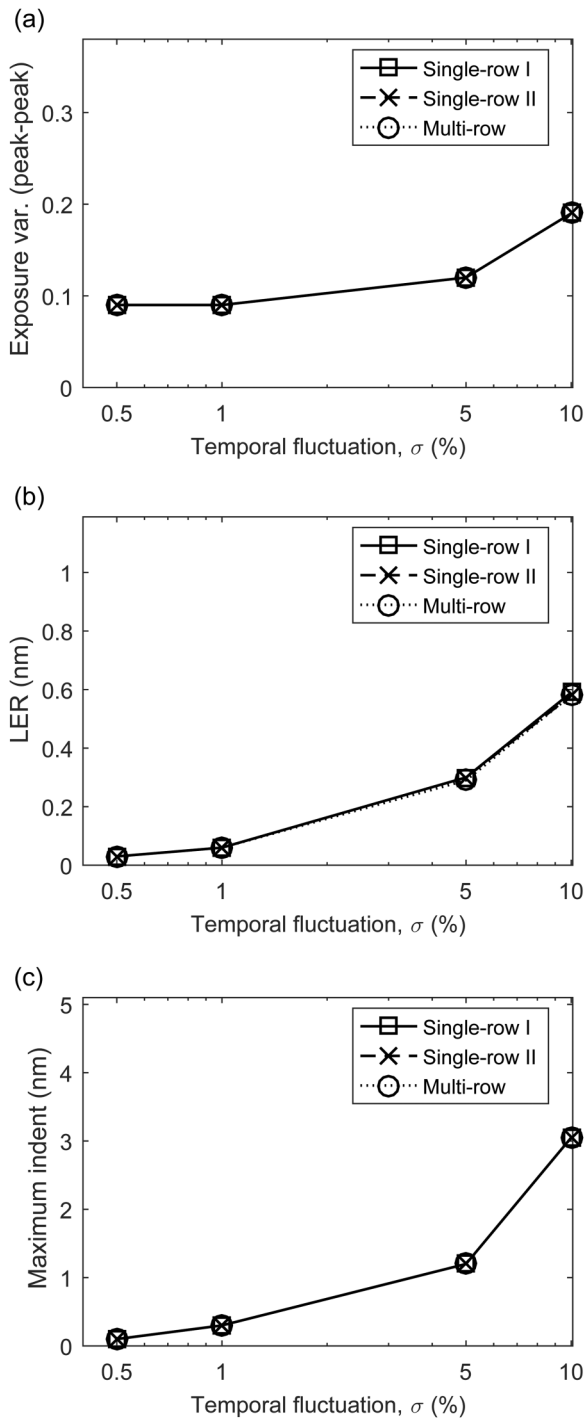

FIG. 17. (a) Exposure variation, (b) LER, and (c) maximum indent with the temporal fluctuation (σ) of beam current varied. $\sigma_t = 2$ nm, $n_f = 0$.

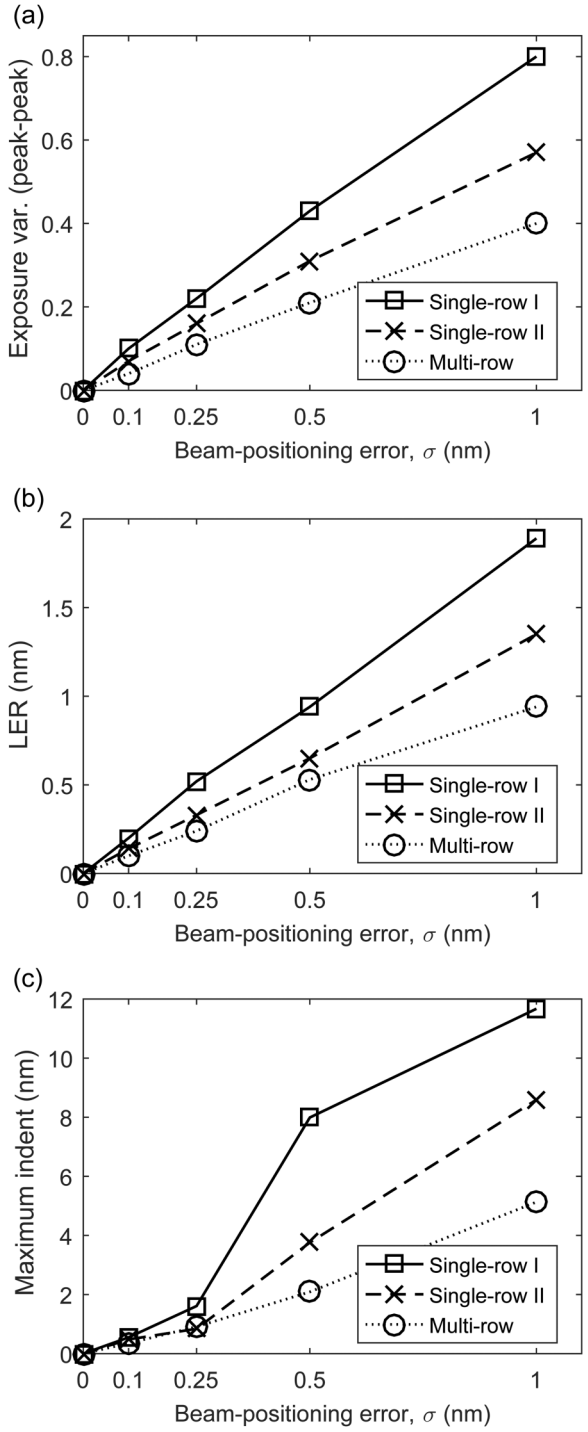

FIG. 18. (a) Exposure variation, (b) LER, and (c) maximum indent with the beam-positioning error (σ) varied. $\sigma_t = 2$ nm, $n_f = 0$.

the quality metrics are improved greatly by the multirow writing method compared to both single-row writing methods. In single-row writing method I, when a beam deviates from its target position, all the shots from that beam received by the affected pixels are out-of-position. In single-row writing method II, the effect of beam-positioning error is averaged among n_g different beams. In the multirow writing method, the level of averaging effect of the beam-positioning error is the highest among the three methods, resulting in the lowest exposure variation, LER, and maximum indent.

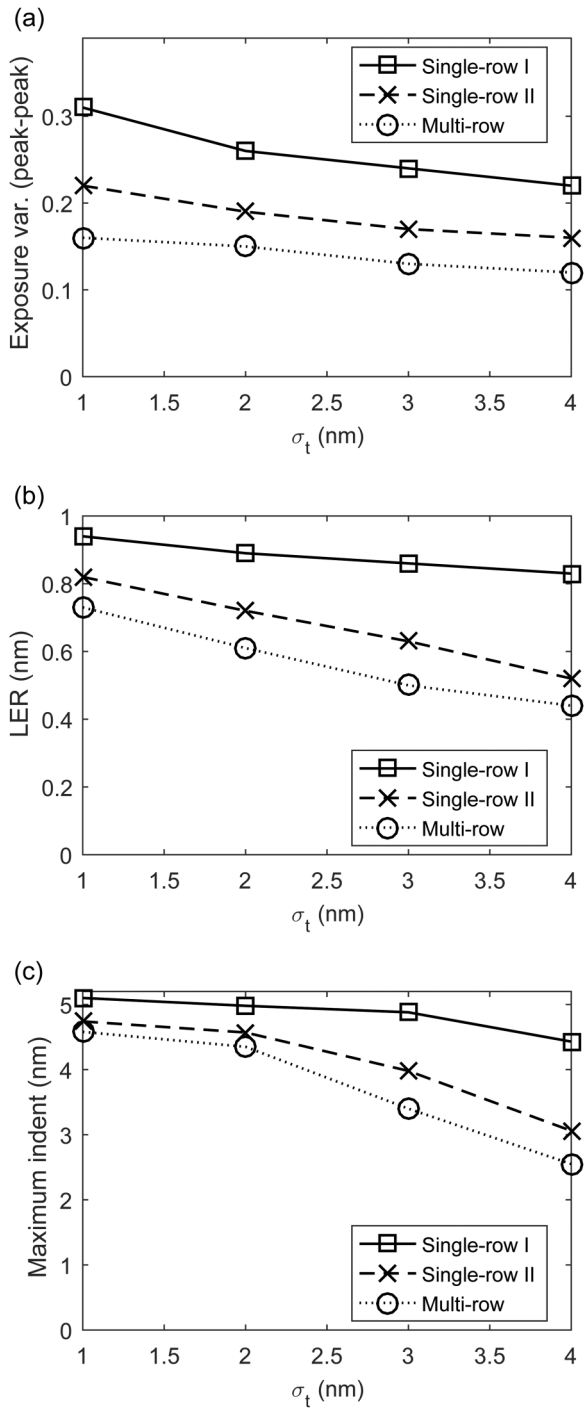

FIG. 19. (a) Exposure variation, (b) LER, and (c) maximum indent with the blurring factor σ_t varied. $n_f = 1$.

G. Dependency on σ_t

All the results so far are for $\sigma_t = 2$ nm. In Fig. 19, the results with σ_t varied are provided for the case when there is one always-off beam with no other abnormalities. The transfer function with a larger σ_t spreads more and drops slower from its maximum. Therefore, when σ_t is larger, the pixels exposed by the always-off beam would receive more exposure contributions from nearby normal shots. Therefore, the quality metrics get improved (reduced) as σ_t increases. The same trend is expected for other abnormalities.

VII. SUMMARY

The major drawback of an e-beam lithographic system has been its low throughput. The use of the recently developed massively-parallel e-beam system would be able to improve the throughput considerably. However, it is unavoidable that some beams on such a system are abnormal, e.g., permanently off or on, spatial and temporal fluctuations of beam current, beam-positioning error, etc. In this study, the negative effects of abnormal beams on the writing qualities are analyzed in terms of the quality metrics such as the exposure variation, line edge roughness, maximum indent, maximum outdent, etc., and the writing methods, single-row writing I, single-row writing II, and multirow writing, are compared. Through an extensive simulation, it has been shown that the multirow writing method always performs better than single-row writing methods I and II. The future study includes the comparison of the multirow writing with the multipass writing method in terms of their effectiveness and overhead since the multipass writing is also able to mitigate the effects of faulty beams by exposing each row of pixels multiple times. The proximity effect correction has been well studied for a long time. But, correcting the proximity effect subject to the constraints of a massively-parallel e-beam system is another interesting problem to be solved.

ACKNOWLEDGMENT

This work was supported in part by a research grant from Samsung Electronics Co., Ltd.

[1]S.-Y. Lee and B. D. Cook, IEEE Trans. Semicond. Manuf. **11**, 117 (1998).
[2]S. J. Wind, P. D. Greber, and H. Rothuizen, J. Vac. Sci. Technol. B **16**, 3262 (1998).
[3]M. Osawa, K. Takahashi, M. Sato, H. Arimoto, K. Ogino, H. Hoshino, and Y. Machida, J. Vac. Sci. Technol. B **19**, 2483 (2001).
[4]S.-Y. Lee, S. C. Jeon, J. S. Kim, K. N. Kim, M. S. Hyun, J. J. Yoo, and J. W. Kim, J. Vac. Sci. Technol. B **27**, 2580 (2009).
[5]Q. Dai, S.-Y. Lee, S.-H. Lee, B.-G. Kim, and H.-K. Cho, J. Vac. Sci. Technol. B **30**, 06F307 (2012).
[6]C. Klein and E. Platzgummer, Proc. SPIE **9985**, 998505 (2016).
[7]C. Klein, H. Loeschner, and E. Platzgummer, J. Micro Nanolithogr. MEMS MOEMS **11**, 031402 (2012).
[8]B. J. Lin, J. Micro Nanolithogr. MEMS MOEMS **11**, 033011 (2012).
[9]H. Matsumoto, H. Inoue, H. Yamashita, H. Morita, S. Hirose, M. Ogasawara, H. Yamada, and K. Hattori, BACUS News **32**, 9 (2016).
[10]P. Petric, C. Bevis, A. Carroll, H. Percy, M. Zywno, K. Standiford, A. Brodie, N. Bareket, and L. Grella, J. Vac. Sci. Technol. B **27**, 161 (2009).
[11]Soomin Moon, S.-Y. Lee, J. Choi, S.-B. Kim, and C.-U. Jeon, J. Vac. Sci. Technol. B **36**, 06JA03 (2018).

[12]H. Fragner and E. Platzgummer, U.S. patent 7777201 B2 (17 August 2010).
[13]S.-Y. Lee, B.-S. Ahn, J. Choi, S.-B. Kim, and C.-U. Jeon, J. Vac. Sci. Technol. B **37**, 061602 (2019).
[14]Q. Dai, R. Guo, S.-Y. Lee, J. Choi, S.-H. Lee, I.-K. Shin, and C.-U. Jeon, Microelectron. Eng. **127**, 86 (2014).
[15]T. Kamikubo, K. Ohtoshi, S. Golladay, V. Katsap, R. Kendall, H. Sunaoshi, and S. Tamamushi, Phys. Procedia **1**, 119 (2008).
[16]S. Johnson, "Simulation of electron scattering in complex nanostructures: Lithography, metrology and characterization," Ph.D. dissertation (Cornell University, 1992).